

MEDICAL INTERPRETABILITY AND KNOWLEDGE MAPS OF LARGE LANGUAGE MODELS

Razvan Marinescu

Lumos AI

razvan@thelumos.ai

Victoria-Elisabeth Gruber

Lumos AI

victoria@thelumos.ai

Diego Fajardo

Lumos AI

diego@thelumos.ai

ABSTRACT

We present a systematic study of medical-domain interpretability in Large Language Models (LLMs). We study how the LLMs both represent and process medical knowledge through four different interpretability techniques: (1) UMAP projections of intermediate activations, (2) gradient-based saliency with respect to the model weights, (3) layer lesioning/removal and (4) activation patching. We present knowledge maps of five LLMs which show, at a coarse-resolution, where knowledge about patient’s ages, medical symptoms, diseases and drugs is stored in the models. In particular for Llama3.3-70B, we find that most medical knowledge is processed in the first half of the model’s layers. In addition, we find several interesting phenomena: (i) age is often encoded in a non-linear and sometimes discontinuous manner at intermediate layers in the models, (ii) the disease progression representation is non-monotonic and circular at certain layers of the model, (iii) in Llama3.3-70B, drugs cluster better by medical specialty rather than mechanism of action, especially for Llama3.3-70B and (iv) Gemma3-27B and MedGemma-27B have activations that collapse at intermediate layers but recover by the final layers. These results can guide future research on fine-tuning, un-learning or de-biasing LLMs for medical tasks by suggesting at which layers in the model these techniques should be applied. We attached our source code to the paper for reproducibility.

1 INTRODUCTION

Large Language Models (LLMs) have achieved impressive performance on a variety of tasks, including for coding, reasoning and in-context learning Radford et al. (2019); Coignion et al. (2024); Hao et al. (2024); Wang et al. (2023); Szymanski et al. (2025); Nguyen et al. (2024). However, the understanding of the underlying mechanisms of how such models represent and store knowledge is still scarce. This is particularly important for medical tasks, where insights about the LLMs’ representations of patient demographics, diseases and drug treatments can help uncover hidden biases, thus making such insights crucial for building safe and trustworthy models.

Over the past few years, a variety of mechanistic interpretability studies have been done on LLMs. A line of research has posited that all features learned by LLMs are linear, a claim known in the field as the *linear representation hypothesis* Bricken et al. (2023); Gurnee & Tegmark (2023); Heinzerling & Inui (2024). However, more recent work has shown that this hypothesis is not always true, and that LLMs can learn non-linear representations of features Engels et al. (2024), such as “days of the week” or “years of a century”, which have circular patterns. Other lines of research have focused on understanding actual modules inside the LLM, such as the attention heads (AHs) Zheng et al. (2024). Thus, attention heads have been found that are specialized in associative memories Bietti et al. (2023), that identify particular structures e.g. the relation between the current token and the previous token Olsson et al. (2022); Nanda et al. (2023) or duplicate words Wang et al. (2022), that perform semantic processing related to the subject of the sentence Chughtai et al. (2024), that

gather context Jin et al. (2024), that perform induction Edelman et al. (2024); Singh et al. (2024); Li et al. (2024); Crosbie & Shutova (2024) as well as other tasks related to latent reasoning and answer preparation, such as ensuring that the answers are correct Wiegreffe et al. (2024), coherent Guo et al. (2024) and faithful to the instructions Tanneru et al. (2024).

While most of interpretability studies have focused on general knowledge and tasks, few works have so far focused on understanding how LLMs represent and process medical knowledge. Some recent studies Chen et al. (2024); Savage et al. (2024) approached medical interpretability by asking the model to explain its diagnosis decisions. He et al. has identified “modular circuits” in a medical-domain LLM (MedLlama-8B), which found certain circuits detect *patient symptoms* regardless of whether the model is doing diagnosis, treatment recommendation, or summarization. Wu et al. (2024) replaced the dense latent vectors of Llama 3 OpenBioLLM-70B with a sparse dictionary of medical features, where each dimension explicitly corresponds to a medical concept. Kraišniković et al. (2025) fine-tuned BERT on a corpus of German pathology reports, and then projected the model’s intermediate activations using t-SNE to visualize clusters of tumor pathologies. However, none of these studies systematically investigated LLM representations across a variety of medical knowledge areas, and in addition each study relied on a single explainability technique. In addition, each study only considered a single LLM. It is thus difficult to draw firm conclusions about the results and whether common representations might emerge across a variety of LLMs.

In this work we present a systematic interpretability analysis of five open-source LLMs (Llama3.3-70B, Gemma3-27B, MedGemma-27B, Qwen-32B and GPT-OSS-120B) for medical tasks. We study how the LLMs store knowledge about patient demographics such as age, as well as medical concepts such as symptoms, diseases, disease progression, drug treatments and drug dosages. We build LLM maps that visualize the layers where such knowledge is stored in the LLM. These maps are built by integrating four independent interpretability methods: (1) UMAP projections of intermediate activations, (2) gradient-based saliency with respect to the model weights, (3) layer lesioning (i.e. removing a layer and measuring the degradation in the response) and (4) activation patching (i.e. replacing the outputs of a single layer with the outputs obtained from a different prompt). We choose these techniques due to their simplicity as well as their significant previous use in the literature McInnes et al. (2018a); Gana et al. (2024); Zhang et al. (2025); Dai et al. (2021). In addition, we find several interesting phenomena: (i) age is encoded in a non-linear manner at intermediate layers in the models, and sometimes shows discontinuities, such as between subjects younger than 18 and those older than 18, (ii) disease progression is circular and hence non-monotonic at certain layers of the model, where late-stage embeddings come closer to the early-stage embeddings (iii) Llama3.3-70B internally has a drug representation that aligns better with medical specialty rather than mechanism of action, (iv) Gemma and MedGemma models have activations that collapse at intermediate layers. The prompts and the medical/drug classifications were verified by a medical professional (Clinical Neuroscience PhD) on our team.

1.1 RELATED WORK

UMAP Embeddings: Zhang et al. (2025) have used UMAP embeddings to visualize intermediate activations in an LLM trained on single-cell RNA data. Bolukbasi et al. (2021); Reif et al. (2019) performed interpretability studies using UMAP on BERT. Yeh et al. (2023) built Attentionviz, a tool for visualizing intermediate embeddings in attention-based models generated using UMAP/t-SNE/PCA.

Weight Saliency: Dai et al. (2021) used a gradient-based saliency method to identify knowledge neurons in pretrained transformers. Fan et al. (2023) used gradient-based weight saliency to un-learn the generation of harmful images. Frankle & Carbin (2018) used weight sparsity, a form of weight saliency, to achieve better generalization in neural network predictions.

Layer and Attention Head Lesioning: In neuroscience, lesioning studies, which involve removing a brain region and studying which cognitive, motor or sensory functions are lost, have successfully identified functions of specific brain regions. In AI interpretability, Logit-Lens *nostalgieberapist* and Tuned-Lens Belrose et al. (2023) were used to interpret models such as GPT-Neo-2.7B by taking intermediate activations at a particular layer and computing the logit directly with it, thus removing all layers after it. Michel et al. (2019) studied BERT outputs after removed one attention head at a time, as well as all-but-one attention heads within a layer. Voita et al. (2019) used layer-wise

relevance propagation Binder et al. (2016) to study the importance of different attention heads before pruning, and they found that only a few specialized heads do the heavy lifting. Zhang et al. (2024) performed a layer ablation study on Llama3-70B and two smaller LLMs and found that only a few layers were important, whereby removing them led to a collapse in the model’s performance. Gromov et al. (2024) removed more and more layers in Llama2, Qwen, Mistral and Phi-2, followed by a small amount of fine-tuning, and found that only by the time 50% of layers were removed did the models’ performance significantly degrade.

Causal interventions and Activation Patching: Causal interventions such as Activation patching Heimersheim & Nanda (2024); Zhang & Nanda (2023) and Rank-One Model Editing (ROME) Meng et al. (2022) have been used to identify circuits in LLMs and transformer-based models, or even functions of specific activation heads Hex. Fierro et al. (2024) used activation patching to localize the role of language during knowledge recall.

2 METHODS

In Fig. 1 we show an overview of our Medical LLM Interpretability study, outlining the process to build LLM maps. We run the LLM through a variety of prompts related to medical knowledge: patient age, symptoms, diseases, drug treatments and drug doses. For each such knowledge area we run four different interpretability methods: (1) UMAP projections of intermediate-layer activations from which we extract quantitative metrics such as Silhouette (cluster separation) scores, (2) gradient-based saliency of model weights (3) layer lesioning, where we replace each layer with the identity function I_n and score the degradation in the altered response, and (4) activation patching, where we replace the outputs of a single layer with the outputs obtained from a different prompt. We finally extract quantitative measures from each of these methods (top-right) and plot the LLM map consisting of the layer intervals where the highest quantitative measures are found. Since each method makes different assumptions and has different strengths and weaknesses, using all of them together helps give confidence that the layers identified are indeed the ones where the medical knowledge is stored in the LLM.

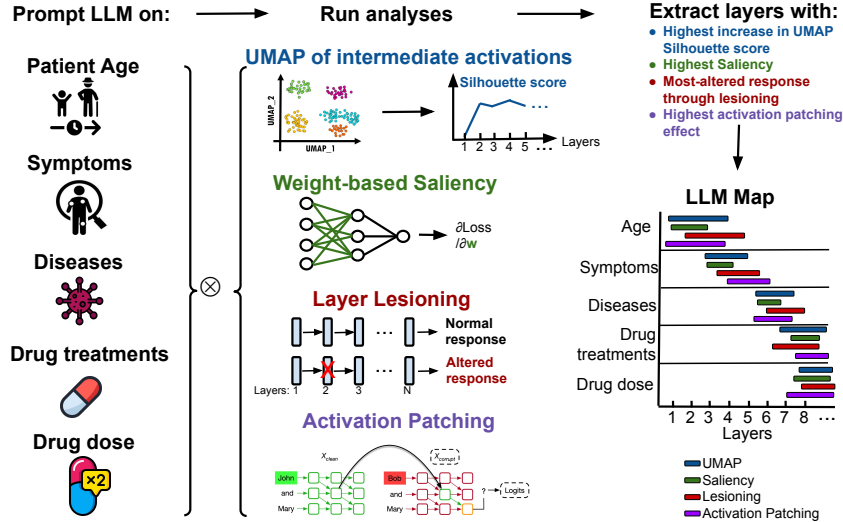


Figure 1: Overview of our Medical LLM Interpretability study, outlining the process to build LLM maps.

UMAP: We use the Uniform Manifold Approximation and Projection (UMAP) McInnes et al. (2018b) to project the intermediate activations of the LLM into a 2D space for visualization. To get a quantitative measure of clustering, we compute the Silhouette Shahapure & Nicholas (2020) (cluster separation) score for each layer, which is a measure of how well the activations cluster in the lower-dimensional space. The Silhouette score is defined as:

$$s(i) = \frac{b(i) - a(i)}{\max(a(i), b(i))} \quad (1)$$

where $a(i)$ is the average distance between i and all other points in the same cluster, and $b(i) = \min_{j \neq i} \frac{1}{n_j} \sum_{x_j \in C_j} d(x_i, x_j)$ is the minimum average distance between i and points in the next closest cluster C_j . To get a per-layer value, we average the Silhouette score across all prompts. We chose Silhouette because it directly measures ground-truth label separability without requiring running a clustering algorithm such as K-means. For the Silhouette score, we project using UMAP on $D = 30$ dimensions (instead of $D = 2$ used for visualization) in order to retain more information about the original datapoints. We further compute confidence intervals for the Silhouette score using bootstrap resampling.

For age-related prompts, which query patients with ages from 1 to 100, we instead compute *local anisotropy*, a measure of “1D-ness” of the datapoints. Taking the 2D UMAP-embeddings, the local anisotropy of a single embedding x_i is defined as $A_i = 1 - \frac{\lambda_2}{\lambda_1}$, where $\lambda_1 \geq \lambda_2$ are the largest two eigenvalues of the local covariance matrix computed from the $k = 20$ nearest neighbors of each point. The final anisotropy value is averaged across all points.

Weight Saliency: We compute the gradient-based saliency of the model weights for each layer by computing $\frac{\partial \log \mathcal{L}}{\partial w}$ where \mathcal{L} is the loss function and w are the model weights. To get a per-layer value, we average the saliency across all weights in the attention heads and MLP at each layer. To obtain more reliable results, we average these values across multiple prompts, and also use these statistics to compute confidence intervals.

Layer Lesioning: We replace each layer in the LLM with the identity function I_n and score the degradation in the altered response. For scoring the degradation, we use an LLM-as-a-judge (here GPT-4o) and use a rubric where a score of 1/10 means no degradation compared to the original response and 10/10 means full degradation with gibberish responses.

Activation Patching: Activation patching is a technique that replaces select internal activations of a neural network model. It runs multiple forward passes: a clean run (cl), a corrupted run ($*$), and a patched run (pt). The patching effect is defined as the gap of the model performance between the corrupted and patched run, under an evaluation metric. For our study, we follow the best practices from Heimersheim & Nanda (2024); Zhang & Nanda (2023). In particular, we only patch the attention heads and the MLP blocks at each layer. We compute the patching effect using the normalized logit difference: $P = \frac{LD_{pt}(r, r') - LD_*(r, r')}{LD_{cl}(r, r') - LD_*(r, r')}$, where $LD(r, r') = \text{Logit}(r) - \text{Logit}(r')$ is the logit difference between responses r and r' (in our case, r and r' are single-token responses such as *Angina* and *Pneumonia* respectively). This normalized value typically lies in the range $[0, 1]$, where 1 signifies fully restored performance after patching and 0 signifies patching has no effect. To obtain more reliable results, we average these values across multiple prompts (see Appendix sec. A), and also use these statistics to compute confidence intervals.

LLM Maps: In order to plot LLM Maps showing where medical knowledge is stored inside the LLM, we select continuous layer intervals from each of the four analyses as follows:

- For UMAP, for all prompt types except age, we select the layer interval showing the highest increase in Silhouette score after Gaussian smoothing ($\sigma = 1.0$), using a sliding window of 3 layers to find the maximum average rate of increase. For age-related prompts, we use local anisotropy instead of Silhouette score.
- For saliency, layer lesioning and activation patching, we select intervals where values are above the 75th percentile threshold after Gaussian smoothing, requiring minimum 2-layer intervals and taking up to 3 intervals per analysis.

We finally plot the LLM map consisting of the layer intervals where the highest quantitative measures are found. Since each method makes different assumptions and has different strengths and weaknesses, using all of them together helps give confidence that the layers identified are indeed the ones where the medical knowledge is stored in the LLM.

3 RESULTS

LLM Medical Maps: In Fig. 2 we show the LLM map for Llama3.3-70B showing where medical knowledge about age, symptoms, diseases, drugs and drug dosages is stored in the LLM. We find that a subject’s age is learned/processed in layers 0-5, medical symptoms are learned in layers 0-9 as well as 15-40. Knowledge about diseases seems to be found in layers 0-5 or potentially 27-37, while knowledge about drugs is most likely learned in layers 15-45. Finally, knowledge about drug dosage is likely learned in the first half of the layers (0-40), although the results seem more inconclusive. For Drug dosage, we could not use the UMAP results due to the lack of a clear quantitative measure that we could compute (see Appendix Fig. 22 for an example plot of UMAP results for drug dosage.)

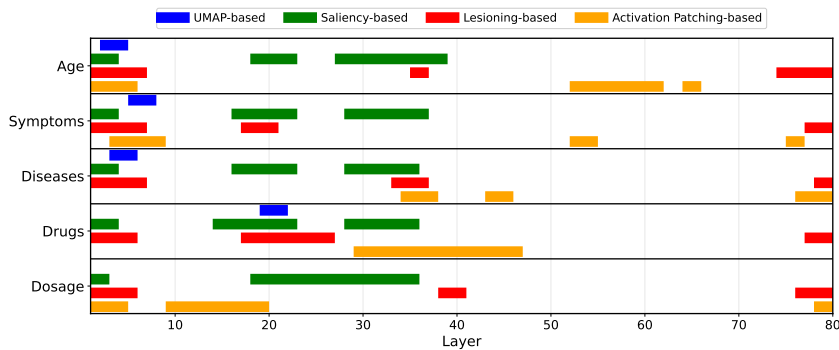


Figure 2: LLM Map for Llama3.3-70B showing where medical knowledge about age, symptoms, diseases, drugs and drug dosages is stored in the model. Each interval shown is estimated quantitatively from four types of analyses: clustering structure in UMAP embeddings, high weight saliency values, high degradation upon layer lesioning/ablation and high patching effect in activation patching.

Age manifold is non-linear: In Fig. 3 we show the UMAP analysis for Llama3.3-70B using prompts about subjects with different ages, broken down by gender. The age manifold is gender-dependent, and further shows non-linearities throughout many intermediate layers, and sometimes altogether a complete change of direction of age progression. In the last plots we plot the true vs predicted age from a linear regression model at layer 37, where the largest discontinuity is found for “she” prompts. Since the discontinuity is between ages 17 and 18, it likely captures a separation between teenagers and adults that the model has learned. A similar age discontinuity between 17 and 18 years is found for “he” and “someone” prompts (results not shown) at the same layer.

Disease Progression representation is circular and non-monotonic: In Fig. 4 we show UMAP-projected intermediate layer activations for Llama3.3-70B using prompts describing the progression of four different diseases: Alzheimer’s disease, Parkinson’s, COVID-19 and COPD. The disease progression manifold shows multiple instances of “circular patterns” across all diseases analyzed. By circular here we mean that the prompts describing late disease stages come back to a closer location to the early-stage prompts. In the penultimate sub-plot we show the closest stages to the first stage (completely healthy with no symptoms), ignoring stage 2, and we find that for many diseases, in particular Parkinson’s and COPD, late stages (5-9) are closer to stage 1 than earlier stages (e.g. 3-4), suggesting that the disease progression is non-monotonic. A similar result is confirmed in the final subplot, where for Alzheimer’s disease in particular stages 2-4 are closer to the end stage (death) than later stages in the representations at many intermediate layers.

Drugs cluster both by mechanism and specialty: In Fig. 5 we show UMAP-projected intermediate layer activations for Llama3.3-70B using prompts about different drugs, broken down by mechanism of action. In Fig. 6, we show similar results for drugs broken down by medical specialty. The LLM learns to represent drugs both by mechanism of action and by medical specialty. Quantitative comparisons with Silhouette Scores (Table 1) confirm that across most models, drugs cluster more by medical specialty than mechanism of action.

For Gemma/MedGemma, activations collapse at intermediate layers: In Fig. 7 we show UMAP-projected intermediate layer activations for Gemma-27B. We notice that the activations collapse in

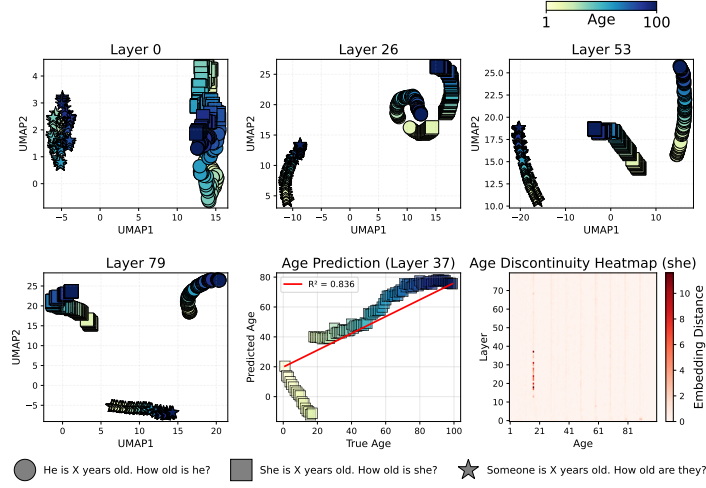


Figure 3: UMAP Analysis using subjects with different ages in Llama3.3-70B. The age manifold shows non-linearities throughout many intermediate layers, as well as a discontinuity between subjects younger than 17 and those 18 or older. Prompts used are shown at the bottom of the figure. The bottom-right plot confirms that the only discontinuity is at age 18.

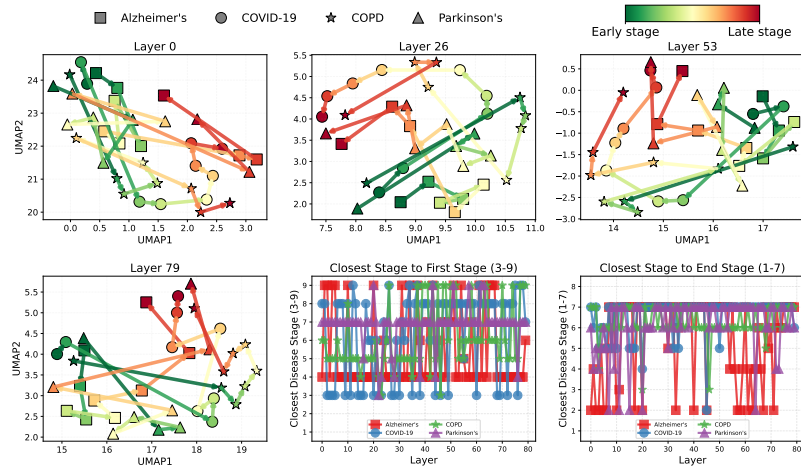


Figure 4: Disease Progression UMAP in Llama3.3-70B. The model shows circular, non-monotonic disease progression, in particular for Alzheimer's disease (stages 2 and 4 are closest to the final stage at many layers) and Parkinson's disease (stage 7 is closest to first stage at most layers). Details about each stage as it was prompted in the model is shown in Appendix Table. 4.

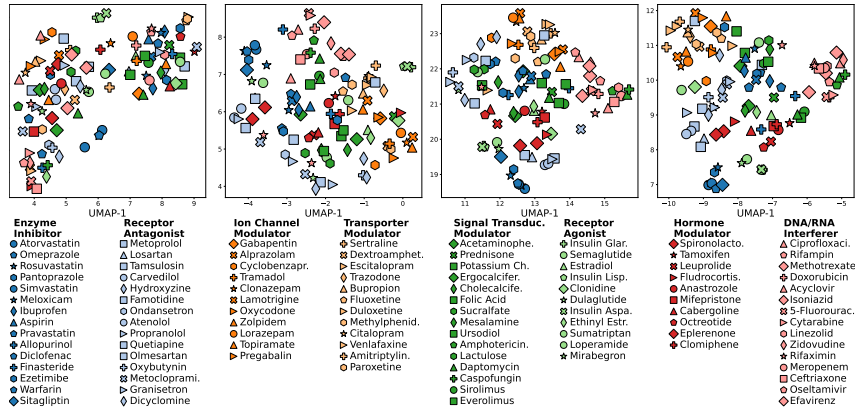


Figure 5: Drug UMAP embeddings colored by mechanism of action in Llama3.3-70B.

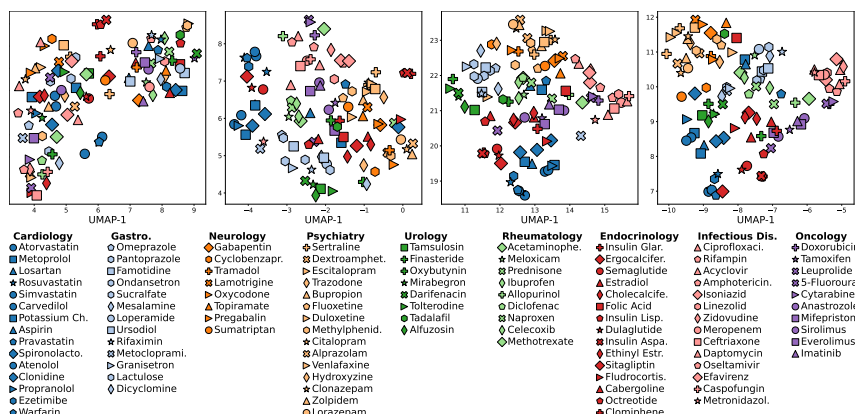


Figure 6: Drug UMAP embeddings colored by medical specialty in Llama3.3-70B

UMAP space at certain intermediate layers (here layer 20 is shown), although they recover in later layers. Results with more intermediate layers are shown in the Appendix section D. We found similar results for MedGemma-27B (see Appendix Fig. 19).

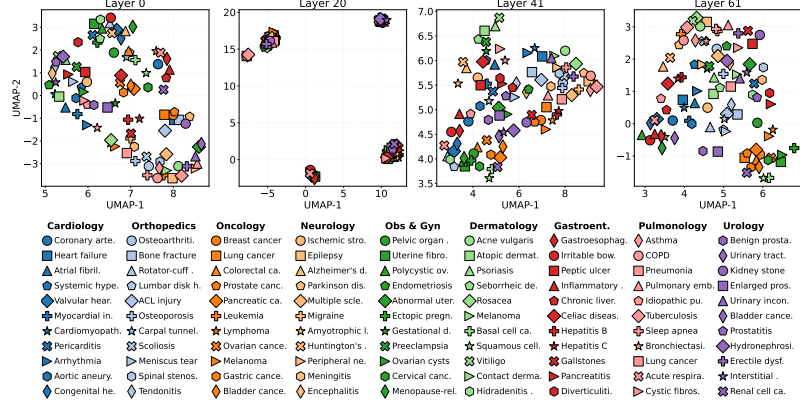


Figure 7: Intermediate layer activations collapse in UMAP space for Gemma (shown above), although they recover in later layers. Similar results are observed for MedGemma. Full results with all layers are shown in the appendix.

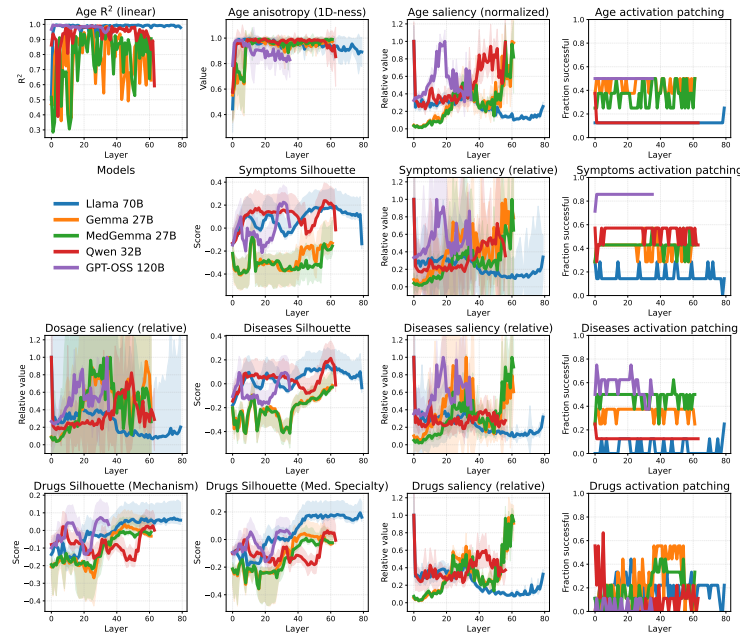


Figure 8: Selected interpretability metrics per layer for the five models. (first row) Age R^2 measuring linearity of age manifold, age anisotropy (a measure of 1D-ness), age gradient-based saliency and fraction of successful activation patches. (second row) medical symptoms metrics, (third row) drug dosage saliency and disease metrics and (fourth row) drug treatment metrics. Lines of some models terminate early due to having a smaller number of layers (e.g. GPT OSS has only 36 layers).

Quantitative interpretability metrics: Across all 5 LLM and all medical areas, we computed key interpretability metrics which we show along with the best layer where these are achieved (Table 1). For Age, we compute a measure of linearity as the R^2 of the linear fit between the true age and the age predicted from a linear fit on the embeddings in the 2D UMAP space. For Symptoms, Diseases and Drugs, we show the Silhouette score, while for disease progression we computed two proxy measures of circularity: (1) the mean μ_{CSFS} of *closest stages to first stage* (CSFS), excluding

stage 2 and (2) the mean μ_{CSLS} of *closest stages to end stage* (CSLS), excluding the penultimate stage. We excluded the second and penultimate stages due to it being affected by the granularity of the disease progression. For Dosages, we show the patching effect as obtained from activation patching. For all metrics, we show the scores obtained at the best layer. We also show the same metrics averaged across all layers (Table 2) and at the last layer (Table 5).

The results show that most models can achieve linear age manifolds at some intermediate layer, even though at the final layer Gemma3-27B and Qwen-32B only achieve an R^2 of around 0.6 (Table 5). The best scores for Silhouette scores are achieved mainly by Llama3.3-70B and Qwen-32B. GPT-OSS-120B also achieves good scores in a variety of categories. MedGemma-27B and Gemma3-27B consistently achieve low scores in all categories except Disease Progression at the final layer.

We further plot key interpretability metrics across all layers for each model (Fig. 8). Llama and GPT show the highest R^2 across layers. Llama and Qwen show the highest UMAP Silhouette scores for symptoms and diseases, while the last layers of Llama show highest UMAP Silhouette scores for drugs. Highest saliencies are observed in the last layers of Gemma/Medgemma, first layer of Qwen, and layers 15-22 of GPT-OSS. Activation patching analyses show that patching succeeded (patching effect > 0.5) more often in GPT and Gemma/Medgemma than in the other models. Layer Lesioning analyses (Appendix Fig. 9) show that removing layers in Gemma/Medgemma seems to lead to severe degradation in the response, while the other models are most robust and thus have redundancy in their layers. Llama and GPT generally show the highest robustness to layer removal, for both early layers and late layers.

Table 1: Per-concept interpretability metrics across models. Values are best layer scores with the layer index. CSFS: Closest Stage to First Stage, CSLS: Closest Stage to Last Stage

Concept	Metric	Llama 70B		Gemma 27B		MedGemma 27B		Qwen 32B		GPT-OSS 120B	
		Score	Layer	Score	Layer	Score	Layer	Score	Layer	Score	Layer
Age	R^2 (linear) \uparrow	1.00 \pm 0.00	3	0.99 \pm 0.00	34	0.98 \pm 0.01	24	0.99 \pm 0.00	25	1.00 \pm 0.00	1
Symptoms	Silhouette \uparrow	0.19 \pm 0.04	63	-0.10 \pm 0.06	12	-0.08 \pm 0.05	12	0.24 \pm 0.05	56	0.23 \pm 0.04	31
Diseases	Silhouette \uparrow	0.16 \pm 0.05	58	-0.01 \pm 0.04	61	-0.03 \pm 0.04	61	0.21 \pm 0.04	60	0.10 \pm 0.05	32
Disease Progression	CSFS \downarrow	3.25 \pm 0.43	11	4.00 \pm 1.22	16	4.00 \pm 1.22	15	3.25 \pm 0.43	13	4.00 \pm 1.73	5
Disease Progression	CSLS \uparrow	7.00 \pm 0.00	78	6.50 \pm 0.87	48	6.25 \pm 0.83	37	7.00 \pm 0.00	62	7.00 \pm 0.00	34
Drugs	Silhouette (mech.) \uparrow	0.07 \pm 0.08	75	0.03 \pm 0.09	45	-0.01 \pm 0.08	44	0.03 \pm 0.06	62	0.07 \pm 0.07	30
Drugs	Silhouette (spec.) \uparrow	0.19 \pm 0.13	78	0.05 \pm 0.12	44	0.01 \pm 0.10	45	0.06 \pm 0.07	58	0.07 \pm 0.07	33
Dosages	Patching Effect \uparrow	2.64 \pm 1.36	79	0.92 \pm 0.61	8	1.71 \pm 1.49	0	7.33 \pm 12.29	0	4.23 \pm 11.04	23

Table 2: Per-concept interpretability metrics across models. Values are mean \pm std across all layers.

Concept	Metric	Llama 70B	Gemma 27B	MedGemma 27B	Qwen 32B	GPT-OSS 120B
Age	R^2 (linear) \uparrow	0.98 \pm 0.06	0.78 \pm 0.16	0.78 \pm 0.18	0.93 \pm 0.09	0.98 \pm 0.01
Symptoms	Silhouette \uparrow	0.08 \pm 0.08	-0.28 \pm 0.09	-0.30 \pm 0.08	0.10 \pm 0.09	-0.02 \pm 0.12
Diseases	Silhouette \uparrow	0.05 \pm 0.07	-0.21 \pm 0.11	-0.22 \pm 0.10	0.04 \pm 0.08	-0.06 \pm 0.09
Disease Progression	CSFS \downarrow	6.17 \pm 1.95	6.10 \pm 2.10	5.95 \pm 2.11	5.73 \pm 1.78	6.22 \pm 1.94
Disease Progression	CSLS \uparrow	6.11 \pm 1.42	4.79 \pm 1.91	4.69 \pm 1.89	6.43 \pm 1.13	5.96 \pm 1.46
Drugs	Silhouette (mech.) \uparrow	-0.01 \pm 0.08	-0.10 \pm 0.09	-0.10 \pm 0.08	-0.08 \pm 0.06	-0.02 \pm 0.07
Drugs	Silhouette (spec.) \uparrow	0.05 \pm 0.13	-0.12 \pm 0.12	-0.14 \pm 0.10	-0.09 \pm 0.07	-0.03 \pm 0.07
Dosages	Patching Effect \uparrow	2.20 \pm 1.17	0.79 \pm 0.70	1.25 \pm 0.85	5.16 \pm 7.84	2.16 \pm 5.77

4 DISCUSSION

The knowledge map we derived for Llama3.3-70B shows that most medical knowledge is stored in the first half of model layers, while the later half of the model likely stores other types of knowledge. However, GPT-OSS-120B and Qwen-32B show an opposite effect, most analyses point to layers in the second half of the model (see appendix sec. C). This suggests that methods trying to finetune these models for medical tasks, or un-learn (Fan et al. (2023)) certain medical biases, should focus on the layers we identified. In addition, our work helps suggest where causal interventions on the models should be focused, in order to change medical concepts.

The non-linearities and discontinuities of the age manifold suggest that age is not learned as a disentangled dimension in the LLM model. This will make age-based re-learning or de-biasing more difficult. In addition, the discontinuities noticed at age 18 suggest that Llama might consider the young subjects in a group of their own, and might display further biases towards that group of

young people in a variety of dimensions. Further investigations are needed to understand exactly what these biases could be.

The circularity of the disease progression manifold is somewhat surprising. Previous research by Engels et al. (2024) has found other types of internal representations that are circular, such as the days of the week of years in a century. While we are not certain about the benefits of such a representation for medical tasks, we hypothesize that a useful representations for disease progression would have three desiderata: (1) it would contain a common healthy state across all diseases, (2) optionally a common death state across all diseases and (3) for certain diseases, the disease progression trajectories would converge at key mid-points; for example, in Alzheimer’s disease, it is hypothesized that both amyloid as well as tau pathology eventually lead to neurodegeneration and brain atrophy, thus the state of neuro-degeneration could be a converging point for both trajectories, eventually leading to advanced cognitive impairment and dementia. While Llama did satisfy (1) and (2) according to our prompts, for (3) we did not find such converging points in our study. However, due to the difficulty of creating suitable prompts, we only did this for a limited number of diseases, so further work needs to be done in order to validate this.

The collapse of intermediate layer activations for Gemma/MedGemma models warrant further investigation. Even though the activations do recover, we believe there is a possibility that representational power is being wasted in those layers where representations collapse. Further investigations are needed to understand the nature of the collapse, whether it is caused by the model’s architecture, the training regime, or the data used for training, and the implications of such a collapse.

Limitations: With lack of ground-truth data, it is difficult to validate the results we derived. In order to alleviate this, we ran four different analyses (UMAP, saliency, layer lesioning and activation patching) on the same model and thus allow the reader to see the consistency of the results across different methods. Since the methods operate with entirely different assumptions, where they are in agreement, we can be significantly more confident in the results we derived. Even when they are not in agreement, some conclusions can still be drawn. For example in the case of drug dosage, both saliency and activation patching indicate signal in the first half of the model layers (even though they disagree on the exact layers), so we can at least draw some broader conclusions even in this case. In addition, as opposed to other interpretability studies, we note that we cannot use human experts to provide ground-truth data due to the lack of understanding of the model’s internal representations.

REFERENCES

Nora Belrose, Zach Furman, Logan Smith, Danny Halawi, Igor Ostrovsky, Lev McKinney, Stella Biderman, and Jacob Steinhardt. Eliciting latent predictions from transformers with the tuned lens. *arXiv preprint arXiv:2303.08112*, 2023.

Alberto Bietti, Vivien Cabannes, Diane Bouchacourt, Herve Jegou, and Leon Bottou. Birth of a transformer: A memory viewpoint. *Advances in Neural Information Processing Systems*, 36: 1560–1588, 2023.

Alexander Binder, Grégoire Montavon, Sebastian Lapuschkin, Klaus-Robert Müller, and Wojciech Samek. Layer-wise relevance propagation for neural networks with local renormalization layers. In *International conference on artificial neural networks*, pp. 63–71. Springer, 2016.

Tolga Bolukbasi, Adam Pearce, Ann Yuan, Andy Coenen, Emily Reif, Fernanda Viégas, and Martin Wattenberg. An interpretability illusion for bert. *arXiv preprint arXiv:2104.07143*, 2021.

Trenton Bricken, Adly Templeton, Joshua Batson, Brian Chen, Adam Jermyn, Tom Conerly, Nick Turner, Cem Anil, Carson Denison, Amanda Askell, et al. Towards monosemanticity: Decomposing language models with dictionary learning. *Transformer Circuits Thread*, 2, 2023.

Junying Chen, Chi Gui, Anningzhe Gao, Ke Ji, Xidong Wang, Xiang Wan, and Benyou Wang. Cod, towards an interpretable medical agent using chain of diagnosis. *arXiv preprint arXiv:2407.13301*, 2024.

Bilal Chughtai, Alan Cooney, and Neel Nanda. Summing up the facts: Additive mechanisms behind factual recall in llms. *arXiv preprint arXiv:2402.07321*, 2024.

Tristan Coignion, Clément Quinton, and Romain Rouvoy. A performance study of llm-generated code on leetcode. In *Proceedings of the 28th international conference on evaluation and assessment in software engineering*, pp. 79–89, 2024.

Joy Crosbie and Ekaterina Shutova. Induction heads as an essential mechanism for pattern matching in in-context learning. *arXiv preprint arXiv:2407.07011*, 2024.

Damai Dai, Li Dong, Yaru Hao, Zhifang Sui, Baobao Chang, and Furu Wei. Knowledge neurons in pretrained transformers. *arXiv preprint arXiv:2104.08696*, 2021.

Abhimanyu Dubey, Abhinav Jauhri, Abhinav Pandey, Abhishek Kadian, Ahmad Al-Dahle, Aiesha Letman, Akhil Mathur, Alan Schelten, Amy Yang, Angela Fan, et al. The llama 3 herd of models. *arXiv e-prints*, pp. arXiv–2407, 2024.

Ezra Edelman, Nikolaos Tsilivis, Benjamin Edelman, Eran Malach, and Surbhi Goel. The evolution of statistical induction heads: In-context learning markov chains. *Advances in neural information processing systems*, 37:64273–64311, 2024.

Joshua Engels, Eric J Michaud, Isaac Liao, Wes Gurnee, and Max Tegmark. Not all language model features are one-dimensionally linear. *arXiv preprint arXiv:2405.14860*, 2024.

Chongyu Fan, Jiancheng Liu, Yihua Zhang, Eric Wong, Dennis Wei, and Sijia Liu. Salun: Empowering machine unlearning via gradient-based weight saliency in both image classification and generation. *arXiv preprint arXiv:2310.12508*, 2023.

Constanza Fierro, Negar Foroutan, Desmond Elliott, and Anders Søgaard. How do multilingual language models remember facts? *arXiv preprint arXiv:2410.14387*, 2024.

Jonathan Frankle and Michael Carbin. The lottery ticket hypothesis: Finding sparse, trainable neural networks. *arXiv preprint arXiv:1803.03635*, 2018.

Bady Gana, Andrés Leiva-Araos, Héctor Allende-Cid, and José García. Leveraging llms for efficient topic reviews. *Applied Sciences*, 14(17):7675, 2024.

Andrey Gromov, Kushal Tirumala, Hassan Shapourian, Paolo Glorioso, and Daniel A Roberts. The unreasonable ineffectiveness of the deeper layers. *arXiv preprint arXiv:2403.17887*, 2024.

Ping Guo, Yubing Ren, Yue Hu, Yanan Cao, Yunpeng Li, and Heyan Huang. Steering large language models for cross-lingual information retrieval. In *Proceedings of the 47th International ACM SIGIR Conference on Research and Development in Information Retrieval*, pp. 585–596, 2024.

Wes Gurnee and Max Tegmark. Language models represent space and time. *arXiv preprint arXiv:2310.02207*, 2023.

Shibo Hao, Yi Gu, Haotian Luo, Tianyang Liu, Xiyan Shao, Xinyuan Wang, Shuhua Xie, Haodi Ma, Adithya Samavedhi, Qiyue Gao, et al. Llm reasoners: New evaluation, library, and analysis of step-by-step reasoning with large language models. *arXiv preprint arXiv:2404.05221*, 2024.

Yinhan He, Wendy Zheng, Yushun Dong, Yaochen Zhu, Chen Chen, and Jundong Li. Towards global-level mechanistic interpretability: A perspective of modular circuits of large language models. In *Forty-second International Conference on Machine Learning*.

Stefan Heimersheim and Neel Nanda. How to use and interpret activation patching. *arXiv preprint arXiv:2404.15255*, 2024.

Benjamin Heinzerling and Kentaro Inui. Monotonic representation of numeric properties in language models. *arXiv preprint arXiv:2403.10381*, 2024.

Stefan Hex. How-to transformer mechanistic interpretability—in 50 lines of code or less! <https://www.lesswrong.com/posts/hnzHrdqn3nrjveayv/how-to-transformer-mechanistic-interpretability-in-50-lines>. Accessed: 2025-09-15.

Zhuoran Jin, Pengfei Cao, Hongbang Yuan, Yubo Chen, Jie Xin Xu, Huaijun Li, Xiaojian Jiang, Kang Liu, and Jun Zhao. Cutting off the head ends the conflict: A mechanism for interpreting and mitigating knowledge conflicts in language models. *arXiv preprint arXiv:2402.18154*, 2024.

Ceca Krašniković, Robert Harb, Markus Plass, Wael Al Zoughbi, Andreas Holzinger, and Heimo Müller. Fine-tuning language model embeddings to reveal domain knowledge: An explainable artificial intelligence perspective on medical decision making. *Engineering Applications of Artificial Intelligence*, 139:109561, 2025.

Ji-An Li, Corey Zhou, Marcus Benna, and Marcelo G Mattar. Linking in-context learning in transformers to human episodic memory. *Advances in neural information processing systems*, 37: 6180–6212, 2024.

Llama-Model-Card. Llama 3 70b model card. <https://build.nvidia.com/meta/llama3-70b/modelcard>, 2024.

Leland McInnes, John Healy, and James Melville. Umap: Uniform manifold approximation and projection for dimension reduction. *arXiv preprint arXiv:1802.03426*, 2018a.

Leland McInnes, John Healy, and James Melville. Uniform manifold approximation and projection for dimension reduction. *arXiv preprint arXiv:1802.03426*, 2018b.

Kevin Meng, David Bau, Alex Andonian, and Yonatan Belinkov. Locating and editing factual associations in gpt. *Advances in neural information processing systems*, 35:17359–17372, 2022.

Paul Michel, Omer Levy, and Graham Neubig. Are sixteen heads really better than one? *Advances in neural information processing systems*, 32, 2019.

Neel Nanda, Senthooran Rajamanoharan, Janos Kramar, and Rohin Shah. Fact finding: Attempting to reverse-engineer factual recall on the neuron level. In *Alignment Forum*, pp. 6, 2023.

Huyen Nguyen, Haihua Chen, Lavanya Pobbathi, and Junhua Ding. A comparative study of quality evaluation methods for text summarization. *arXiv preprint arXiv:2407.00747*, 2024.

nostalgia. Interpreting gpt: the logit lens. <https://www.lesswrong.com/posts/AcKRB8wDpdaN6v6ru/interpreting-gpt-the-logit-lens>. Accessed: 2025-09-15.

Catherine Olsson, Nelson Elhage, Neel Nanda, Nicholas Joseph, Nova DasSarma, Tom Henighan, Ben Mann, Amanda Askell, Yuntao Bai, Anna Chen, et al. In-context learning and induction heads. *arXiv preprint arXiv:2209.11895*, 2022.

Alec Radford, Jeffrey Wu, Rewon Child, David Luan, Dario Amodei, Ilya Sutskever, et al. Language models are unsupervised multitask learners. *OpenAI blog*, 1(8):9, 2019.

Emily Reif, Ann Yuan, Martin Wattenberg, Fernanda B Viegas, Andy Coenen, Adam Pearce, and Been Kim. Visualizing and measuring the geometry of bert. *Advances in neural information processing systems*, 32, 2019.

Thomas Savage, Ashwin Nayak, Robert Gallo, Ekanath Rangan, and Jonathan H Chen. Diagnostic reasoning prompts reveal the potential for large language model interpretability in medicine. *NPJ Digital Medicine*, 7(1):20, 2024.

Ketan Rajshekhar Shahapure and Charles Nicholas. Cluster quality analysis using silhouette score. In *2020 IEEE 7th international conference on data science and advanced analytics (DSAA)*, pp. 747–748. IEEE, 2020.

Aaditya K Singh, Ted Moskovitz, Felix Hill, Stephanie CY Chan, and Andrew M Saxe. What needs to go right for an induction head? a mechanistic study of in-context learning circuits and their formation. *arXiv preprint arXiv:2404.07129*, 2024.

Annalisa Szymanski, Noah Ziems, Heather A Eicher-Miller, Toby Jia-Jun Li, Meng Jiang, and Ronald A Metoyer. Limitations of the llm-as-a-judge approach for evaluating llm outputs in expert knowledge tasks. In *Proceedings of the 30th International Conference on Intelligent User Interfaces*, pp. 952–966, 2025.

Sree Harsha Tanneru, Dan Ley, Chirag Agarwal, and Himabindu Lakkaraju. On the difficulty of faithful chain-of-thought reasoning in large language models. In *Trustworthy Multi-modal Foundation Models and AI Agents (TiFA)*, 2024.

Elena Voita, David Talbot, Fedor Moiseev, Rico Sennrich, and Ivan Titov. Analyzing multi-head self-attention: Specialized heads do the heavy lifting, the rest can be pruned. *arXiv preprint arXiv:1905.09418*, 2019.

Kevin Wang, Alexandre Variengien, Arthur Conmy, Buck Shlegeris, and Jacob Steinhardt. Interpretability in the wild: a circuit for indirect object identification in gpt-2 small. *arXiv preprint arXiv:2211.00593*, 2022.

Liang Wang, Nan Yang, and Furu Wei. Learning to retrieve in-context examples for large language models. *arXiv preprint arXiv:2307.07164*, 2023.

Sarah Wiegreffe, Oyvind Tafjord, Yonatan Belinkov, Hannaneh Hajishirzi, and Ashish Sabharwal. Answer, assemble, ace: Understanding how transformers answer multiple choice questions. *arXiv e-prints*, pp. arXiv–2407, 2024.

John Wu, David Wu, and Jimeng Sun. Dila: Dictionary label attention for mechanistic interpretability in high-dimensional multi-label medical coding prediction. *arXiv preprint arXiv:2409.10504*, 2024.

Catherine Yeh, Yida Chen, Aoyu Wu, Cynthia Chen, Fernanda Viégas, and Martin Wattenberg. Attentionviz: A global view of transformer attention. *IEEE Transactions on Visualization and Computer Graphics*, 30(1):262–272, 2023.

Fred Zhang and Neel Nanda. Towards best practices of activation patching in language models: Metrics and methods. *arXiv preprint arXiv:2309.16042*, 2023.

Haotian Zhang, Yu H Sun, Wenxing Hu, Xu Cui, Zhengyu Ouyang, Derrick Cheng, Xinmin Zhang, and Baohong Zhang. Comppbioagent: An llm-powered agent for single-cell rna-seq data exploration. *bioRxiv*, pp. 2025–03, 2025.

Yang Zhang, Yanfei Dong, and Kenji Kawaguchi. Investigating layer importance in large language models. *arXiv preprint arXiv:2409.14381*, 2024.

Zifan Zheng, Yezhaohui Wang, Yuxin Huang, Shichao Song, Mingchuan Yang, Bo Tang, Feiyu Xiong, and Zhiyu Li. Attention heads of large language models: A survey. *arXiv preprint arXiv:2409.03752*, 2024.

APPENDIX

Notes on LLM usage: We used LLMs for the following:

- For brainstorming ideas, such as on how to implement the hooks for activation patching and lesioning
- For generating portions of our code, such as specific functions, and for debugging
- For auto-completions during the writing of the latex file, mainly for latex code generation for tables and figures
- For generating some of the prompts used in the analyses, which we then manually reviewed and edited

A PROMPTS USED

Table 3: Prompt templates used across all analyses. Blue words are automatically substituted with a variety of values in order to test multiple ages, symptoms, diseases, drugs and drug dosages. Green words denote the expected answers with respect to which we compute gradients (saliency) or logit differences (activation patching).

Analysis	Prompt Templates
Age	
UMAP	He is {20} years old.
Saliency	Answer with a single number, nothing else. At what age is someone legally considered an adult? {18}
Lesioning	How long do people live around the world?
Activation Patching	Clean: A {75}-year-old patient has {memory problems}. The most likely cause is ...{Dementia} Corrupt: A {5}-year-old patient has {memory problems}. The most likely cause is ...{Epilepsy}
Symptoms	
UMAP	A patient has {headache}.
Saliency	Answer with a single word. What is the main symptom present in {Pneumonia}? {headache}
Lesioning	A patient has a lupus. What symptoms are associated with this disease?
Activation Patching	Clean: For {migraine}, a common symptom is ...{headache} Corrupt: For {epilepsy}, a common symptom is ...{seizures}
Diseases	
UMAP	A patient was diagnosed with {COPD}.
Saliency	A patient has fever, productive cough, and chest crackles on exam. The most likely diagnosis is ...{Pneumonia}
Lesioning	A 30-year-old female patient presents with chronic cough, shortness of breath, and wheezing. What is the most likely diagnosis?
Activation Patching	Clean: A patient has {chest pain and shortness of breath}. The most likely diagnosis is ...{Angina} Corrupt: A patient has {chest pain and coughing}. The most likely diagnosis is ...{Pneumonia}
Drugs	
UMAP	A patient takes {Atorvastatin}.
Saliency	Answer with a single word only, describing a drug. A patient suffers from high LDL cholesterol and has atherosclerotic disease. What drug should the patient take? {Atorvastatin}
Lesioning	A patient takes Metformin. What are the side effects?
Activation Patching	Clean: The patient has {ADHD}. A common medication is ...{Adderall} Corrupt: The patient has {depression}. A common medication is ...{Sertraline}
Drug Dosage	
UMAP	A patient took {5}mg of {Amlodipine}.
Saliency	A patient has taken {5} mg of {Amlodipine}. Will the patient be alive or dead? {alive}, {dead}
Lesioning	What is a safe dose of Amlodipine and what is a lethal dose?
Activation Patching	Clean: What will happen to the patient? Answer in exactly one English word: stable or dead. A patient took {5}mg of {Amlodipine}. The patient will be ...{stable} Corrupt: Same as the clean prompt, except the dose changed to {100}mg, and expected answer changed to {dead}

Table 4: Disease progression prompts used for UMAP analysis. Each disease has 9 stages from healthy to death, showing realistic progression patterns.

Disease	Progression Prompts
Alzheimer's Disease	
Stage 1	Someone is healthy with no symptoms.
Stage 2	Someone occasionally worries about minor forgetfulness.
Stage 3	Someone frequently misplaces items and struggles with recent memory.
Stage 4	Someone forgets recent conversations and repeats questions.
Stage 5	Someone struggles significantly with language and daily tasks.
Stage 6	Someone regularly becomes confused and has trouble recognizing family.
Stage 7	Someone has severe cognitive decline and is unable to communicate clearly.
Stage 8	Someone is bedridden, minimally responsive, after severe cognitive decline.
Stage 9	Someone just died from severe cognitive decline.
COVID-19	
Stage 1	Someone is healthy with no symptoms.
Stage 2	Someone has mild fatigue.
Stage 3	Someone has mild fatigue, slight fever, dry cough.
Stage 4	Someone has persistent cough, fever, mild shortness of breath.
Stage 5	Someone has worsening respiratory distress, oxygen saturation 90%.
Stage 6	Someone has been receiving supplemental oxygen and is in the ICU.
Stage 7	Someone was sedated, intubated and mechanically ventilated.
Stage 8	Someone experienced multi-organ failure and declining vital signs.
Stage 9	Someone just died from multi-organ failure and declining vital signs.
COPD	
Stage 1	Someone is healthy with no symptoms.
Stage 2	Someone experiences shortness of breath with strenuous exercise.
Stage 3	Someone experiences shortness of breath when climbing stairs, mild cough.
Stage 4	Someone is breathless during everyday tasks, chronic cough.
Stage 5	Someone has regular flare-ups, struggles with daily tasks.
Stage 6	Someone requires frequent hospitalizations due to breathing difficulty.
Stage 7	Someone needs supplemental oxygen at home, has severe breathlessness.
Stage 8	Someone experiences chronic respiratory failure, continuous oxygen dependence.
Stage 9	Someone just died from chronic respiratory failure, continuous oxygen dependence.
Parkinson's Disease	
Stage 1	Someone is healthy with no symptoms.
Stage 2	Someone has mild tremors in one hand.
Stage 3	Someone experiences stiffness and slowness of movement.
Stage 4	Someone has mild difficulty with balance and coordination.
Stage 5	Someone has moderate difficulty with balance and coordination.
Stage 6	Someone has severe tremors and muscle rigidity.
Stage 7	Someone is unable to walk without assistance.
Stage 8	Someone is bedridden with severe motor impairment and requires full-time care.
Stage 9	Someone just died from severe motor impairment and complications.

B ADDITIONAL PERFORMANCE METRICS

Table 5: Per-concept interpretability metrics across models. Values are scores at the last layer (representations right before output).

Concept	Metric	Llama 70B	Gemma 27B	MedGemma 27B	Qwen 32B	GPT-OSS 120B
Age	R^2 (linear) \uparrow	0.98 ± 0.02	0.63 ± 0.07	0.90 ± 0.06	0.59 ± 0.37	0.98 ± 0.00
Symptoms	Silhouette \uparrow	-0.14 ± 0.05	-0.13 ± 0.07	-0.16 ± 0.07	-0.01 ± 0.04	0.01 ± 0.05
Diseases	Silhouette \uparrow	-0.03 ± 0.04	-0.01 ± 0.04	-0.03 ± 0.04	-0.01 ± 0.05	-0.04 ± 0.03
Disease Progression	CSFS \downarrow	7.25 ± 1.09	5.50 ± 2.60	5.50 ± 2.60	6.50 ± 0.87	5.50 ± 2.06
Disease Progression	CSLS \uparrow	6.50 ± 0.50	4.75 ± 2.28	4.75 ± 2.28	5.75 ± 1.09	5.50 ± 2.06
Drugs	Silhouette (mech.) \uparrow	0.06 ± 0.08	-0.03 ± 0.09	-0.01 ± 0.08	0.00 ± 0.06	0.03 ± 0.07
Drugs	Silhouette (spec.) \uparrow	0.16 ± 0.13	-0.03 ± 0.12	-0.02 ± 0.10	-0.01 ± 0.07	0.04 ± 0.07
Dosages	Patching Effect \uparrow	2.64 ± 1.36	0.67 ± 0.82	0.98 ± 0.63	5.77 ± 9.05	2.40 ± 3.64

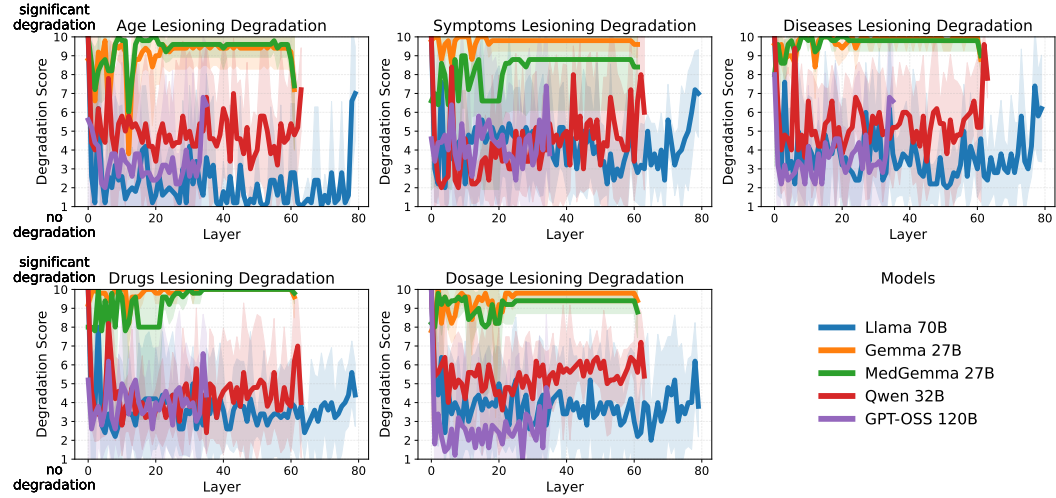


Figure 9: Lesioning metrics per layer.

C MAIN LLM MAPS FOR ALL OTHER MODELS

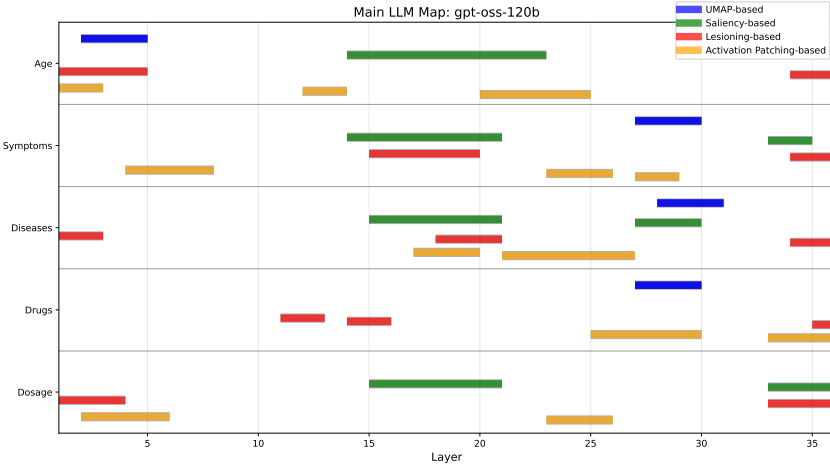


Figure 10: LLM Medical Map for GPT-OSS-120B



Figure 11: LLM Medical Map for Qwen-32B

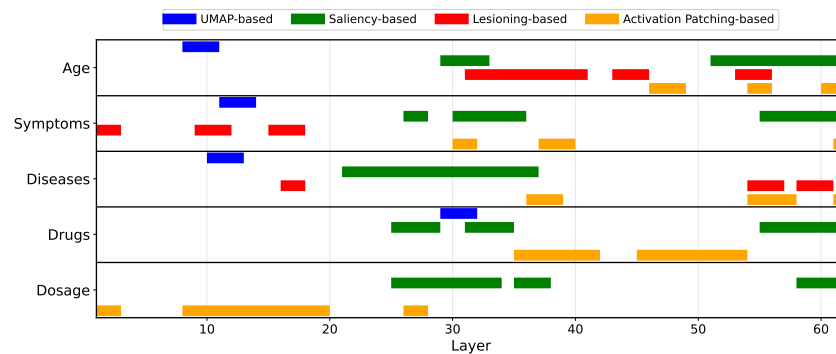


Figure 12: LLM Medical Map for Gemma3-27B

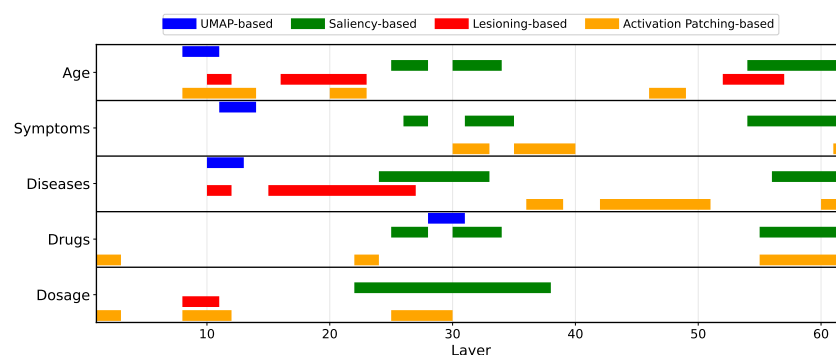


Figure 13: LLM Medical Map for MedGemma-27B

D FULL PLOTS FOR ALL KEY RESULTS IN MAIN PAPER

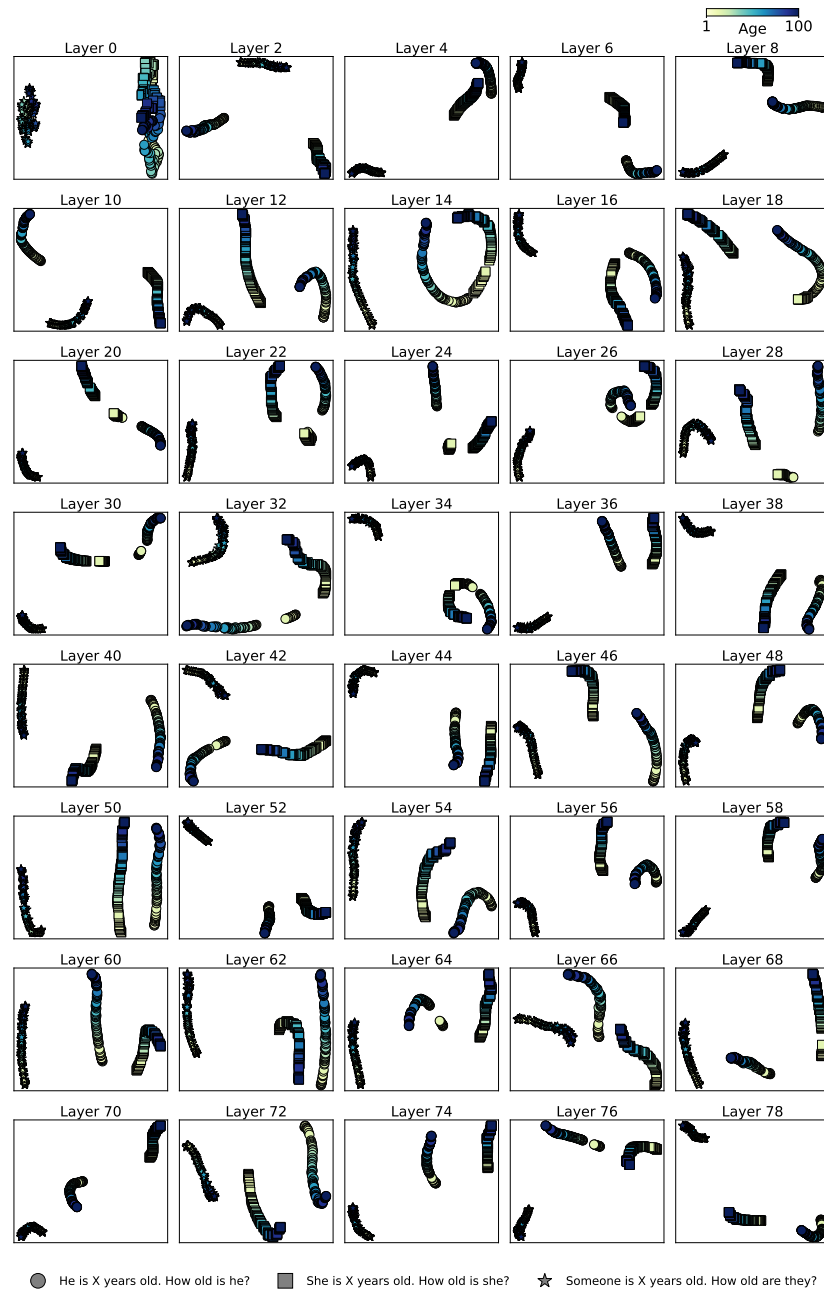


Figure 14: UMAP Analysis for Llama3.3-70B using prompts about subjects with different ages. The age manifold shows non-linearities throughout many intermediate layers (e.g. layer 8). Prompts used are shown at the bottom of the figure.

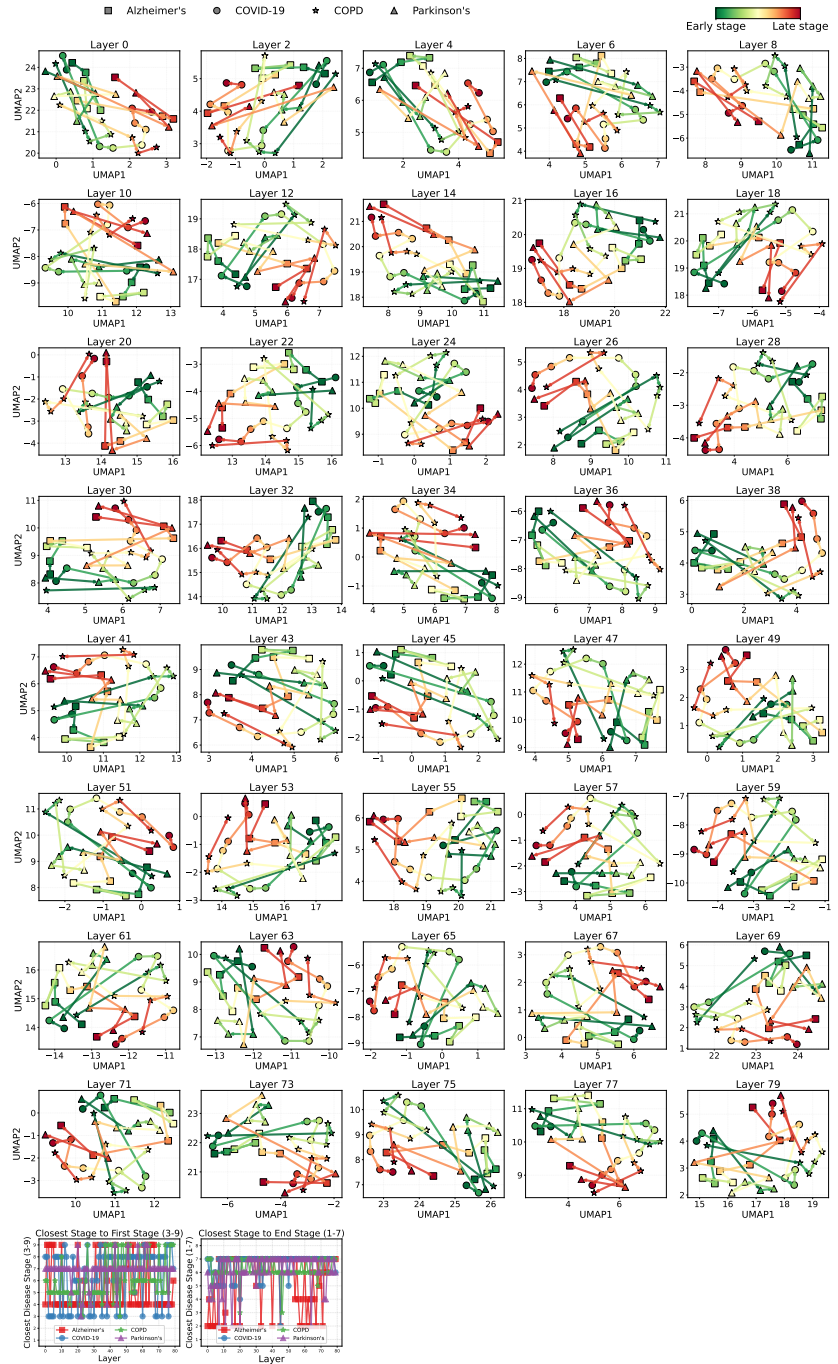


Figure 15: UMAP embeddings for disease progression for Llama3.3-70B .

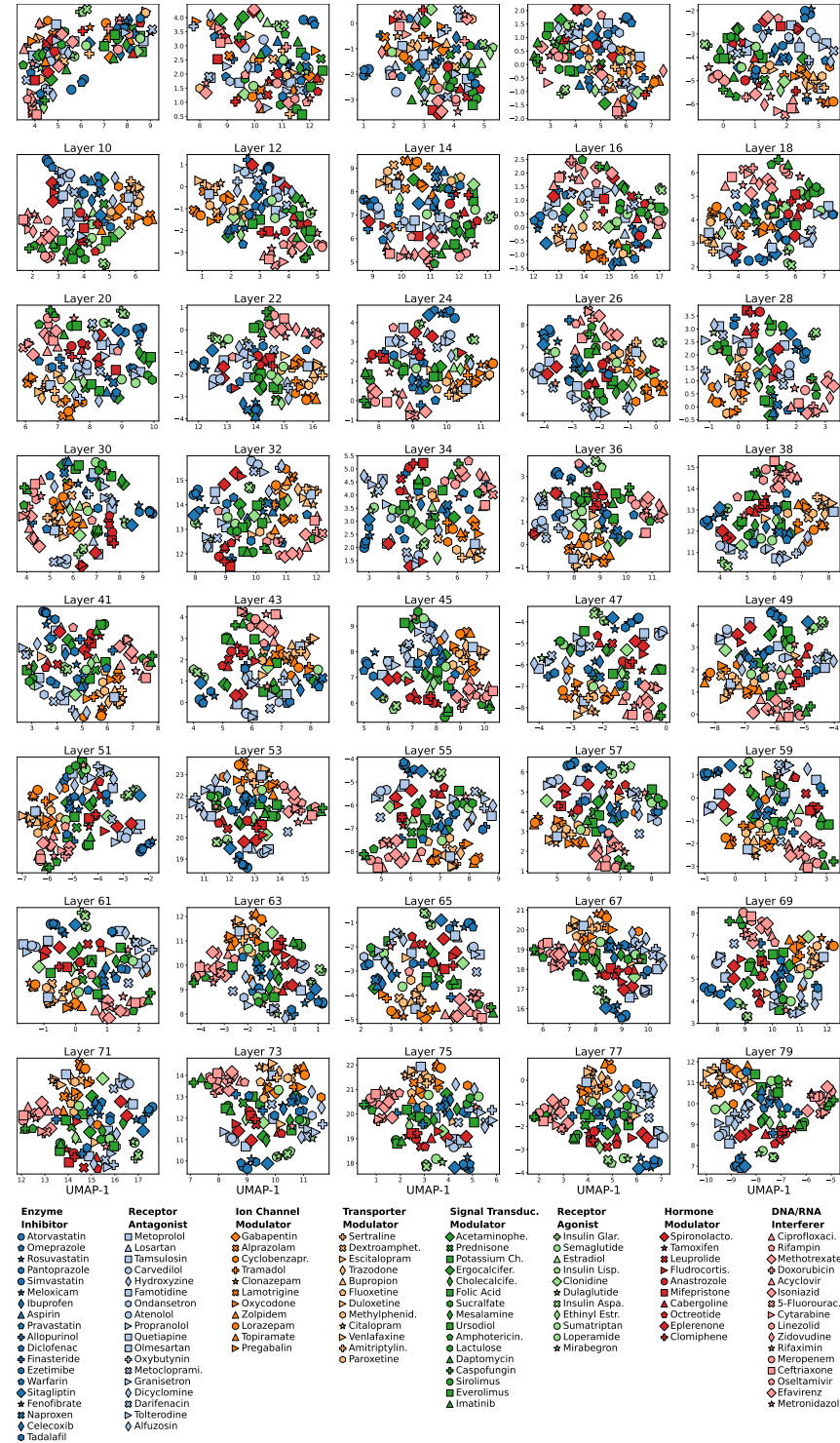


Figure 16: Drug UMAP embeddings by mechanism of action in Llama3.3-70B

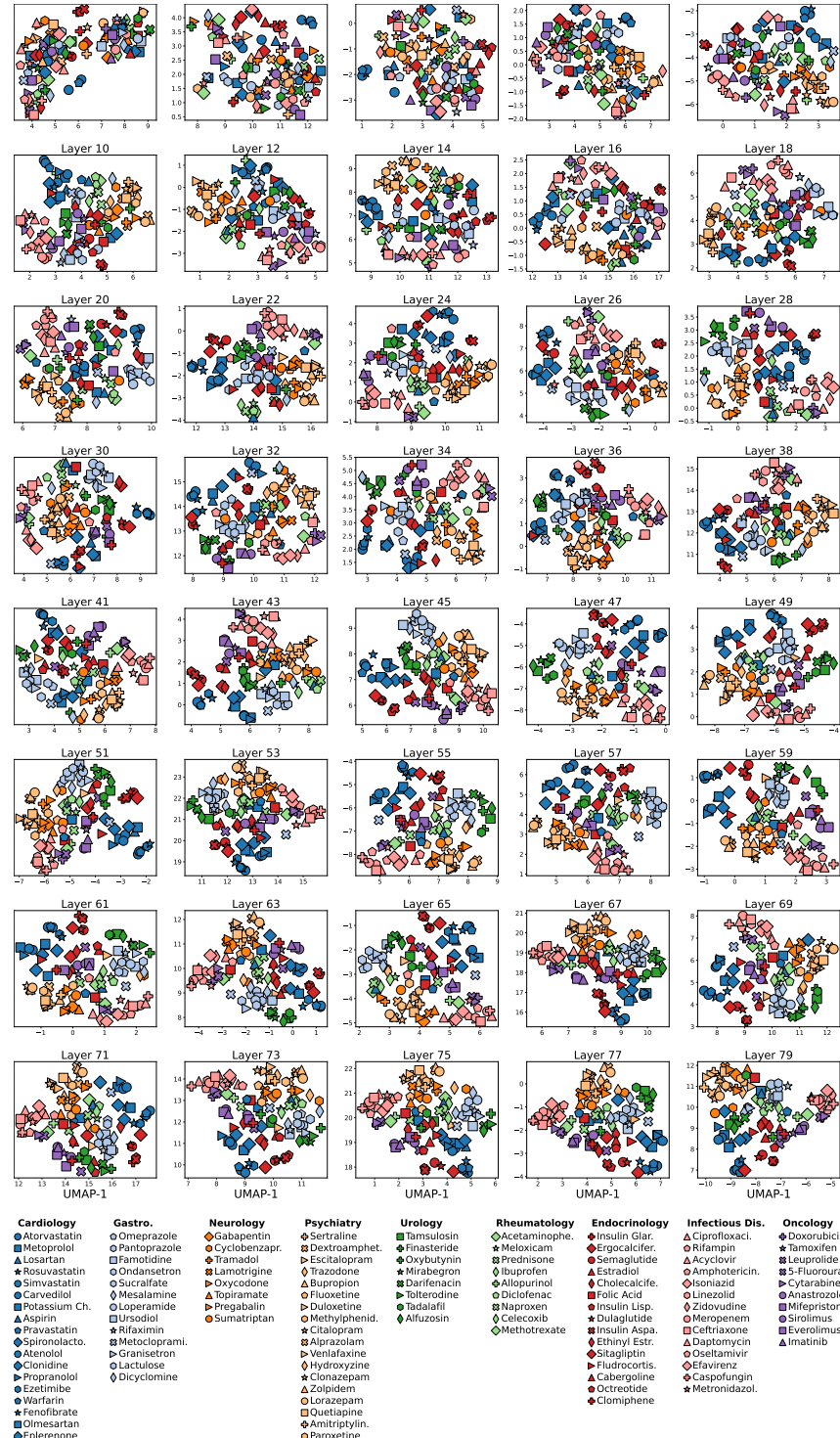


Figure 17: Drug UMAP embeddings by medical specialty in Llama3.3-70B

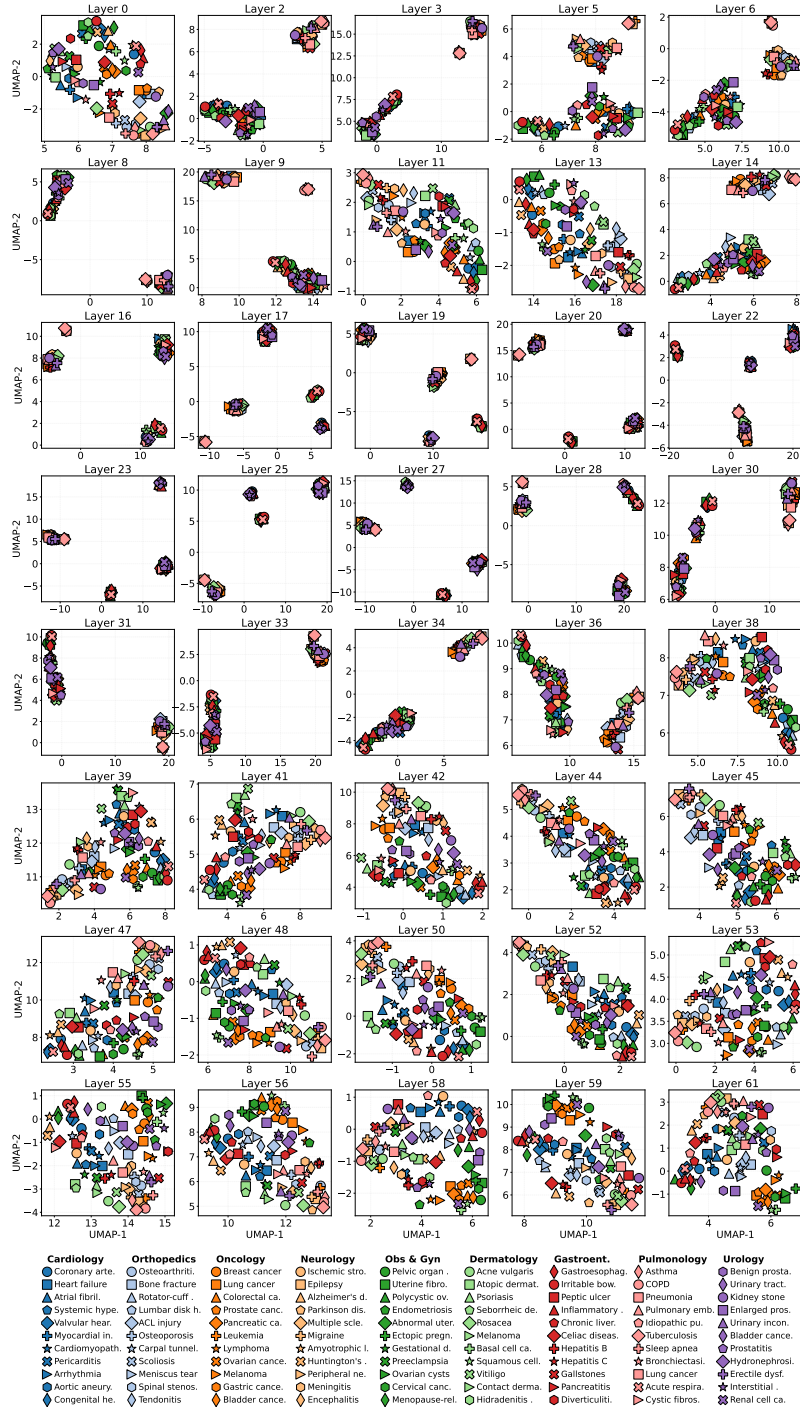


Figure 18: Intermediate layer activations collapse in UMAP space for Gemma.

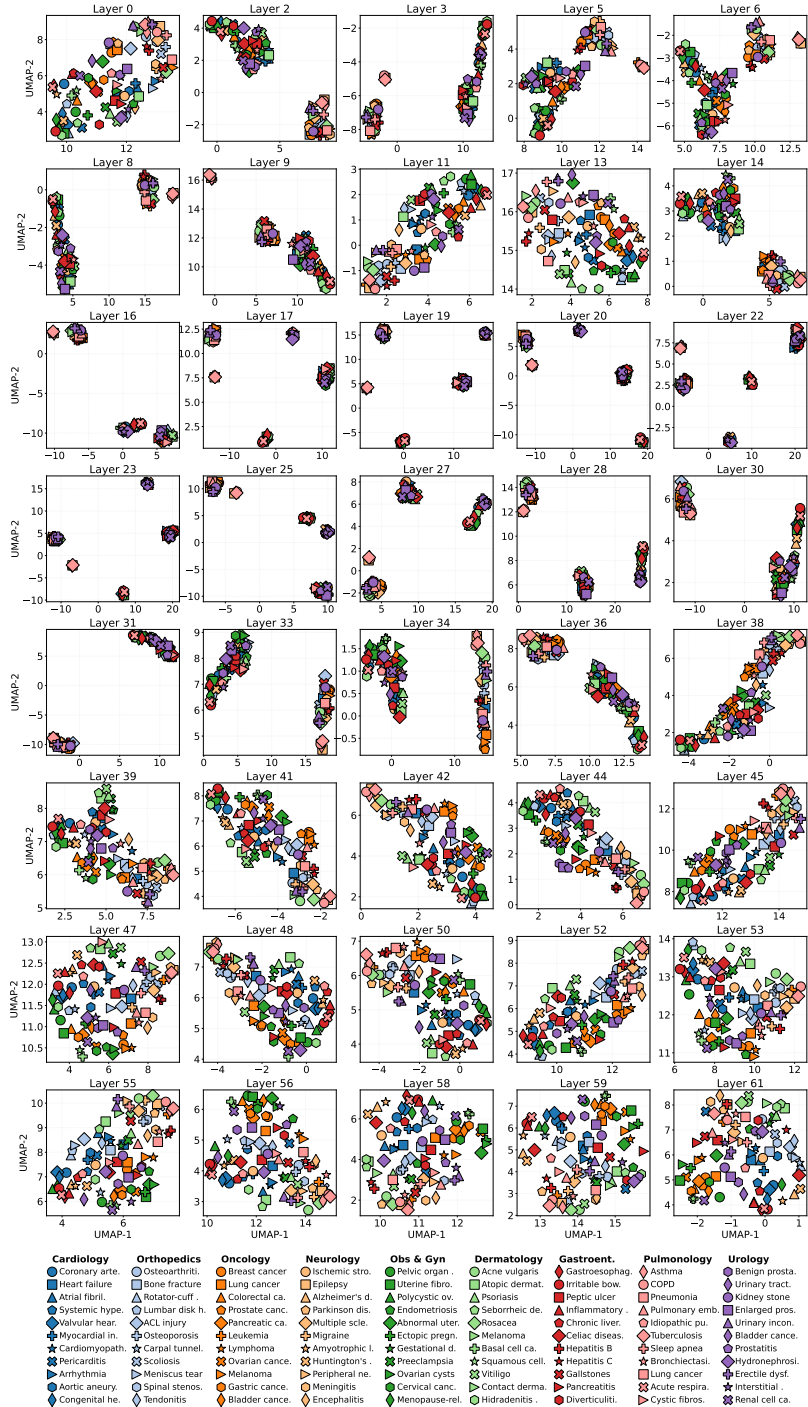


Figure 19: Intermediate layer activations collapse in UMAP space for MedGemma.

E OTHER UMAP RESULTS ON LLAMA3.3-70B

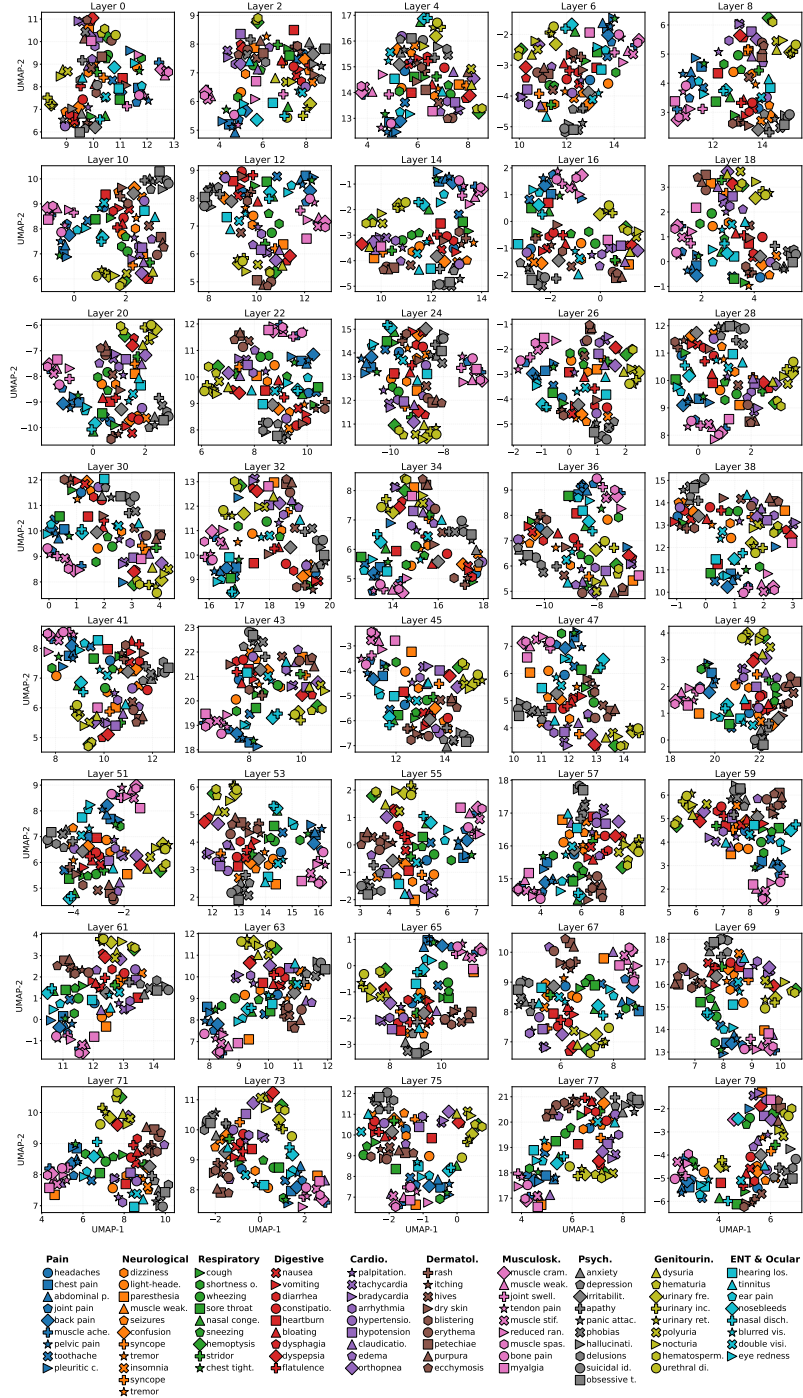


Figure 20: Symptom UMAP embeddings for Llama3.3-70B coloured by symptom groups.

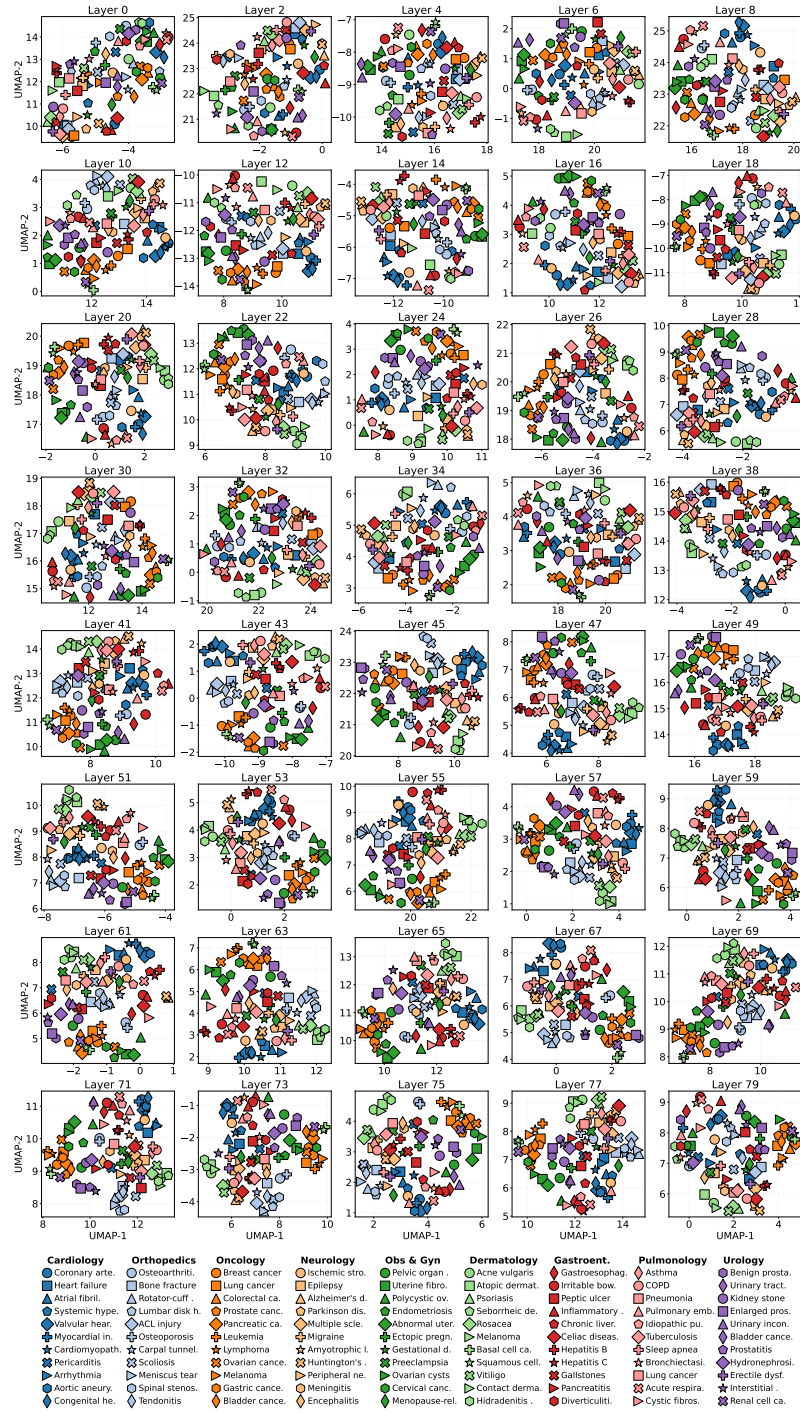


Figure 21: Disease UMAP embeddings for Llama3.3-70B coloured by medical specialties.

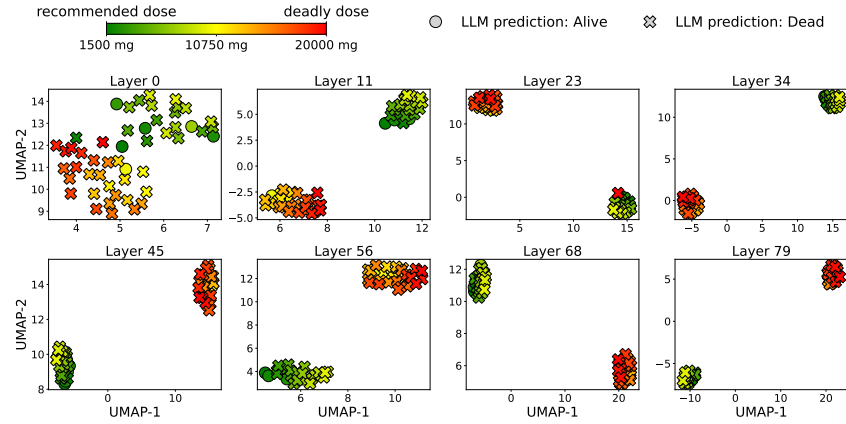


Figure 22: UMAP Analysis for Llama3.3-70B using prompts about different drug dosages for Potassium Chloride. We ran 50 prompts with different drug dosages between the recommended dose (1,500mg) and a deadly dose of 20,000mg. We also analyzed the Llama’s response to each dose, and classified it as alive or dead. Two groups are forming early on in the internal representation of the LLM, but these are not aligned with alive/dead groups. We don’t understand this behaviour, and further research is needed to look into this.

F LLAMA3.3-70B

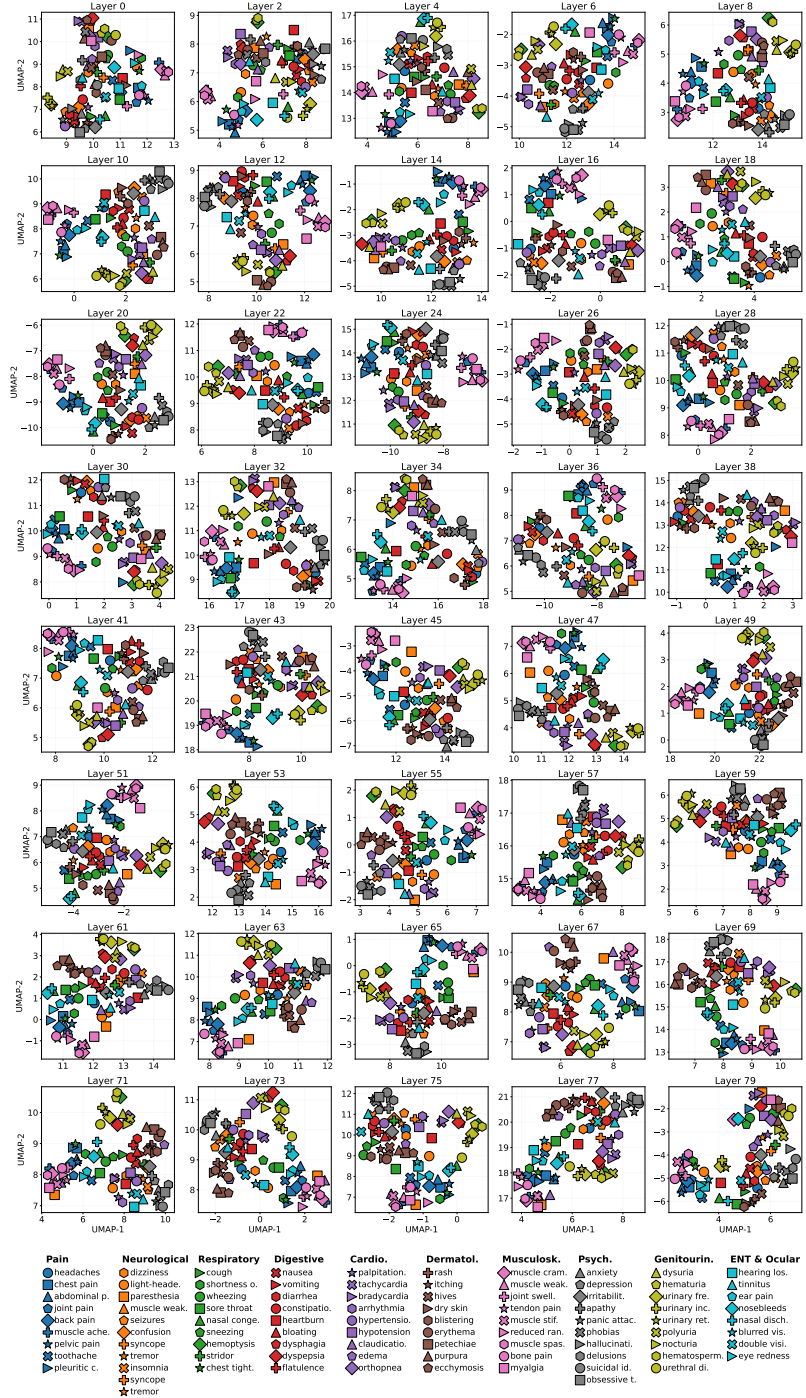


Figure 23: UMAP Analysis for Llama3.3-70B using prompts about different symptoms.

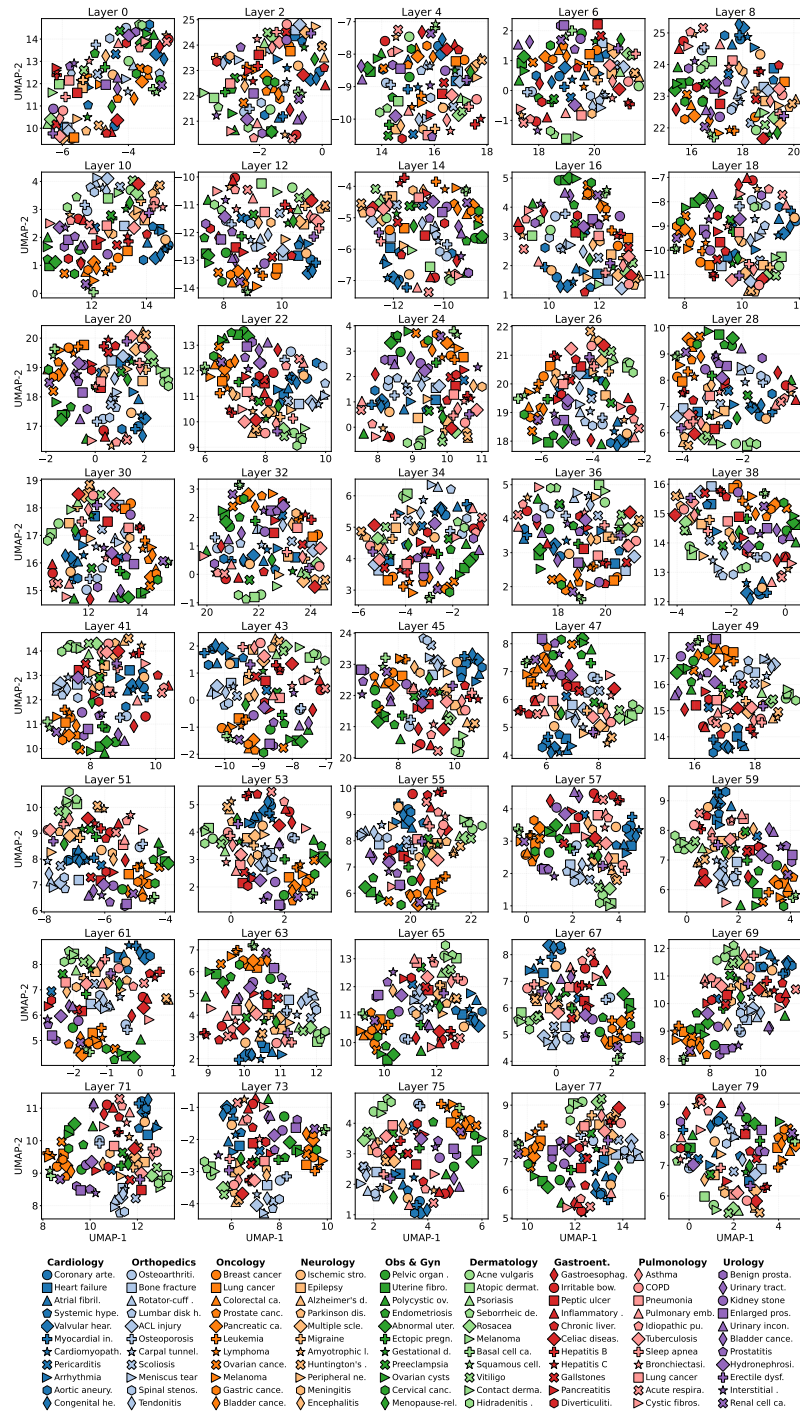


Figure 24: UMAP Analysis for Llama3.3-70B using prompts about different diseases.